Suzaku/Fermi Challenges to Relativistic Jets in AGN

J. Kataoka[1], R. K. Sato[2], and G. M. Madejski[3],
on behalf of the Fermi-LAT collaboration

[1] Research Institute for Science and Engineering, Waseda University, Sinjuku, Tokyo 169-8555, Japan
[2] Institute of Space and Astronautical Science/JAXA, Sagamihara, Kanagawa 229-8510, Japan
[3] KIPAC/Stanford Linear Accelerator Center, Stanford University, Stanford, CA 94-305, USA
E-mail(JK): kataoka.jun@waseda.jp

Abstract

In next five years, dramatic progress is anticipated for the AGN studies, as we have two important missions to observe celestial sources in the high energy regime: Fermi and Suzaku. Simultaneous monitoring observations by the two instruments (Fermi-LAT and Suzaku XIS/HXD) will be particularly valuable for variable radio-loud AGN, allowing the cross-correlations of time series as well as detailed modeling of the spectral evolution between the X-ray and gamma-ray energy bands. In this paper, we particularly focus on the results from recent Suzaku X-ray observations of five flat-spectrum radio quasars (FSRQs), simultaneously observed with Fermi. Our aim is to reveal the nature of high-energy emission of luminous blazars in their quiescent/low-activity states covering the frequency range from 10^{14} Hz up to 10^{25} Hz.

Key words: AGN: blazars, Fermi, Suzaku, Swift, multiwavelength monitoring

1. Introduction

Observationally, blazar class includes flat-spectrum radio quasars (FSRQs) and BL Lac objects. FSRQs have strong and broad optical emission lines, while the lines are weak or absent in BL Lacs. During the first three months of the Fermi Large Area Telescope's (LAT) all-sky-survey, 132 bright sources at Galactic latitudes ($|b| > 10^\circ$) were detected at a confidence level greater than $10\,\sigma$ (Abdo et al. 2009a). As expected from the EGRET observations, a large fraction (106) of these sources have been identified with known AGNs (Abdo et al. 2009b). This includes two radio galaxies (Centaurus A and NGC 1275; Abdo et al. 2009c) and 104 blazars consisting of 58 FSRQs, 42 BL Lac objects, and 4 blazars with unknown classification.

In order to understand the blazar phenomenon and the differences between BL Lacs and FSRQs, as well as the origin of spectral transitions in a particular object, one has to obtain truly simultaneous coverage across the entire spectrum, during both flaring and quiescent states. However, past γ-ray observations in quiescent states have been limited to only a few extremely luminous objects, such as PKS 0528-134 or 3C 279. Only now, with the successful launch of the Fermi satellite and the excellent performance of the Suzaku instruments, do we have an opportunity to study high-energy spectra of blazars with substantially improved sensitivity, and therefore the different states of the sources' activity.

In this paper, we report the high-sensitivity, broadband Suzaku observations of five FSRQs, namely PKS 0208-512, Q 0827+243, PKS 1127-145, PKS 1510-089, and 3C 454.3. Additionally, all of these sources were monitored simultaneously or quasi-simultaneously by the Fermi LAT and Swift Ultraviolet/Optical Telescope (UVOT; Roming et al. 2005). These broadband and high-sensitivity observations allow us to reveal the characteristic of the high-energy inverse Compton (IC) continuum in the quiescent states of luminous blazars. A full detailed description is given in Abdo et al. (2009d; corresponding author R.K.Sato), but here, due to lack of space, only several highlights from Suzaku observations are discussed.

2. Observation and Data Reduction

2.1. Suzaku

Five FSRQs were observed by Suzaku for 40 ks each as one of the long-category projects between 2008 October and 2009 January. All of the sources were focused on the nominal center position of the XIS detector. For the XIS, we analyzed the screened data, reduced via Suzaku software version 2.0. The HXD/PIN data (version 2.0) were processed with basically the same screening criteria as those for the XIS. We used the response files, version ae_hxd_pinhxdnom5_20080716.rsp, provided by the HXD team.

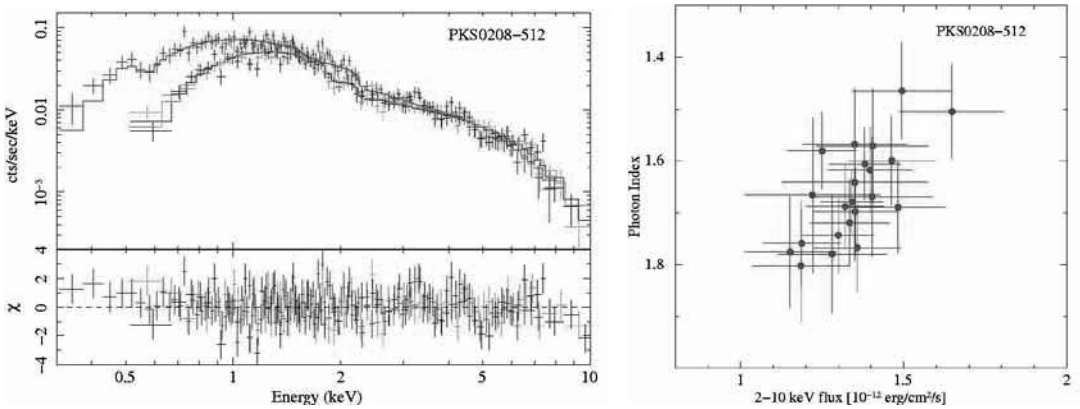

Fig. 1. *left*: Suaku XIS spectrum of PKS 0208-512. *right*: Correlation of the 2-10 keV flux vs. photon index.

2.2. Swift UVOT

Four analyzed FSRQs (PKS 0208-512, Q 0827+243, PKS 1510-089, and 3C 454.3) were observed with Swift between 2008 October and 2009 January, as part of Swift "target of opportunity" observations. We analyzed the data taken within or near the time of the Suzaku observations. The UVOT observing mode commonly takes an exposure in each of the six optical and ultraviolet filters (v, b, u, uvw1, uvm2, and uvw2) per Swift pointing. Level 2 sky-corrected image data were used. The background was extracted from a nearby source-free circular region with 15″ radius. All image data were corrected for coincidence loss. The observed magnitudes were converted into flux densities by the standard procedures (Poole et al. 2008).

2.3. Fermi-LAT

We analyzed the LAT's observations of the five blazar regions using data collected during the first 4-5 months centered around Suzaku observations. Little variability indicated by the LAT lightcurves for the studied objects during this time implies that the constructed broad-band spectra, even though not exactly simultaneous, are representative for the low-activity states of all five blazars. We use the "Diffuse" class events (Atwood et al. 2009), which are those reconstructed events having the highest probability of being photons. Science Tools version v9r14 and IRFs (Instrumental Response Functions) P6_V3 (a model of the spatial distribution of photon events calibrated pre-launch) were used.

3. Results

3.1. Suzaku

3.1.1. PKS 0208-512

The power-law model with the Galactic value $N_{\rm H} = 3.08 \times 10^{20}\,{\rm cm}^{-2}$ for the XISs spectra of PKS 0208-512 gives $\Gamma = 1.68 \pm 0.02$ and the $2-10$ keV flux $F_{2-10{\rm keV}} = (1.37 \pm 0.03) \times 10^{-12}\,{\rm erg\,cm}^{-2}\,{\rm s}^{-1}$, but the residuals of the fits show moderate excess feature at low energies, below 1 keV (Figure 1 (*left*)). In the previous observation with BeppoSAX during a high flux state (Tavecchio et al. 2002; $F_{2-10{\rm keV}} \sim 4.7\times10^{-12}\,{\rm erg\,cm}^{-2}\,{\rm s}^{-1}$), the X-ray spectrum is well described by a power-law with photon index $\Gamma \sim 1.7$, but the spectrum was heavily absorbed below 1 keV, indicating $N_{\rm H} = 1.67 \times 10^{21}\,{\rm cm}^{-2}$. The variable soft X-ray emission of PKS 0208-512 may indicate that the convex spectrum observed by BeppoSAX reflects an intrinsic IC continuum shape, while the soft excess observed by Suzaku reflects the presence of an additional spectral component which becomes prominent when the source gets fainter (see Kataoka et al. 2008). Interestingly, soft excess can be well represented by thermal emission of $kT = 0.092 \pm 0.003$ keV.

In order to investigate the X-ray spectral evolution, we divided the total exposure into one-orbit intervals. We fitted the overall XIS spectra between 0.3 and 10 keV with an absorbed simple power-law function. Figure 1 (*right*) shows a relation between the $2-10$ keV fluxes versus the photon indices for the case of PKS 0208-512. Significant spectral variation was also seen in Q 0827+243 ($\Gamma = 1.2 - 1.6$), PKS 1127-145 ($\Gamma = 1.4 - 1.6$), and PKS 1510-089 ($\Gamma = 1.3 - 1.5$). This clearly reveals a spectral evolution with the X-ray spectra hardening as the sources become brighter.

3.1.2. 3C 454.3

In the case of 3C 454.3 we obtained the best fit to the XISs and HXD/PIN spectra assuming an absorbed power-law model with a photon index of $\Gamma = 1.61 \pm 0.01$ and a column density of $N_{\rm H} = (9.07 \pm 0.35) \times 10^{20}\,{\rm cm}^{-2}$, which is larger than the Galactic value at the 99.9% confidence level. The unabsorbed $2 - 10$ keV flux is $F_{2-10{\rm keV}} = (1.66 \pm 0.01) \times 10^{-11}\,{\rm erg\,cm}^{-2}\,{\rm s}^{-1}$. In addition, we reanalyzed the previous Suzaku data collected in December 2007 during the high state. The time averaged XISs and HXD/PIN spectra was well described by a single absorbed power-law model with

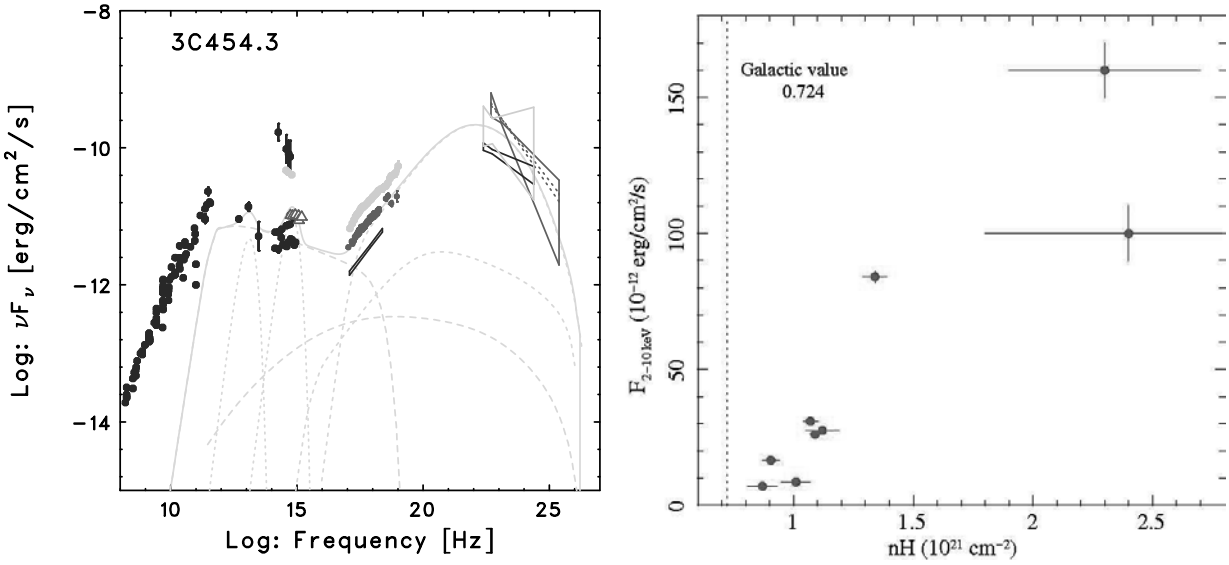

Fig. 2. *left*: Overall SED of 3C 454.3 (Suzaku, Swift and Fermi). *right*: N_H vs. 2-10 keV flux for different observations of 3C 454.3.

$\Gamma = 1.64 \pm 0.01$, implying the flux $F_{2-10\mathrm{keV}} = (3.09 \pm 0.02) \times 10^{-11}\,\mathrm{erg\,cm^{-2}\,s^{-1}}$, which is larger by a factor of two than the one found in our 2008 observations. The absorption column also shows a higher value of $N_{\mathrm{H}} = (1.07 \pm 0.03) \times 10^{21}\,\mathrm{cm^{-2}}$.

3.2. Fermi

To study the average spectra of five objects during the four or five months of observations, we use the standard maximum-likelihood spectral estimator provided with the LAT science tools GTLIKE. Photons were extracted from a region with a 10° radius centered on the coordinates of the position of each object. We subtracted the Galactic diffuse emission by using specific maps based on the GALPROP model with the normalization free to vary in the fit.

We model the continuum emission from each source with a single power-law. The extragalactic background is assumed to have a power-law spectrum, with its spectral index and the normalization free to vary in the fit. From an unbinned GTLIKE fit the best fit photon indices are $\Gamma = 2.33 \pm 0.05$ for PKS 0208-512, $\Gamma = 2.62 \pm 0.35$ for Q 0827+243, $\Gamma = 2.77 \pm 0.14$ for PKS 1127-145, $\Gamma = 2.48 \pm 0.03$ for PKS 1510-089, and $\Gamma = 2.51 \pm 0.02$ for 3C 454.3. Here only statistical errors are taken into account, and the spectra were extrapolated down to 100 MeV. In the case of bright sources (PKS 1510-089 and 3C 454.3), we also analyzed the data collected during the Suzaku observing period to construct the simultaneous broad-band spectra spectra.

4. Discussion and Conclusion

4.1. Broad-Band Spectral Fits

We constructed the broad-band spectral energy distribution (SED) ranging from the radio to γ-ray bands for five observed FSRQs. An example SED of 3C 454.3 is given in Figure.2 (*left*). Here we just summarize our conclusion from the model fitting. First, the LAT fluxes are dominated by the IC/BLR (broad line region) component, while in the X-ray band both IC/BLR and IC/DT (dusty torus) processes may be comparable. In addition, the SSC emission seems negligible, being in particular too weak to account for the soft X-ray excess discussed in the previous sections. This excess, on the other hand, may be well represented by the high-energy tail of the synchrotron continuum, or an additional blackbody-type spectral component.

Second, some of the obtained jet parameters for five analyzed luminous blazars in their quiescent/low-activity states are significantly different from the analogous parameters claimed for the flaring states (even in the same object). For example, in the case of the high-activity state of PKS 1510-089, Kataoka et al. (2008) estimated the total kinetic power of the jet as $L_j \sim 2.7 \times 10^{46}\,\mathrm{erg\,s^{-1}}$, which is larger than the one evaluated in this paper by a factor of about 30. In addition, our model values of the jet bulk Lorentz factors are also systematically lower than the ones given in the literature ($\Gamma_j \simeq 10$ versus 20). Interestingly, the other jet parameters are comparable to the ones found for flaring FSRQs.

Hence, we feel secure to conclude that the low- and high-activity states of luminous blazar sources are due to the low and high total kinetic power of the jet, respec-

tively, possibly related to lower and higher bulk Lorentz factors within the blazar emission zone. And indeed, keeping in mind highly dynamical and complex jet formation processes in the closest vicinities of supermassive black holes, shaped by notoriously unstable accretion of the jet fuel, such a significant variation in the total kinetic output of the outflow should not be surprising. Further support for this scenario comes from the fact that the jet efficiency factors estimated here are significantly lower than the ones found for powerful blazars in their flaring states (see Sambruna et al. 2006, Ghisellini et al. 2009).

4.2. Spectral Evolution

As shown in § 3.1.1, the X-ray spectra of the analyzed FSRQs flattens with increasing flux. The electrons emitting X-ray photons in these sources are very low-energy, so cooling effects cannot play any role in the observed spectral evolution. Adiabatic losses, if present, should not result in changing the slope of the power-law X-ray continua as well. Thus, one may suspect that the revealed spectral changes are shaped by the acceleration process within the blazar emission zone. The above interpretation, on the other hand, would imply a significant variability in the γ-ray frequency range. Indeed, the broken power-law form of the electron energy distribution revealed by our spectral modeling discussed in the previous section implies the γ-ray flux $F_\gamma \equiv [\nu F_\nu]_\gamma$ around the IC spectral peak $\nu_\gamma \sim 10^{22}\,\mathrm{Hz}$ to be roughly

$$F_\gamma \simeq F_X \left(\frac{\nu_\gamma}{\nu_X}\right)^{2-\Gamma} \simeq 10^{4\,(2-\Gamma)} F_X\,, \qquad (1)$$

where F_X is the monochromatic X-ray flux measured around $\nu_X \sim 10^{18}\,\mathrm{Hz}$, and Γ is the observed X-ray photon index. For example, our analysis for PKS 0208-512 indicates a photon index of $\Gamma_1 \sim 1.8$ for an X-ray flux $F_{X,\,1} \sim 1.2 \times 10^{-12}\,\mathrm{erg\,cm^{-2}\,s^{-1}}$ in the lower state, and $\Gamma_2 \sim 1.5$ for $F_{X,\,2} \sim 1.6 \times 10^{-12}\,\mathrm{erg\,cm^{-2}\,s^{-1}}$ in the higher state.

Thus, if the observed X-ray variability is due to flattening of the electron energy distribution during the acceleration process, one should observe the γ-ray variability of the order of

$$\frac{F_{\gamma,\,2}}{F_{\gamma,\,1}} \simeq 10^{4\,(\Gamma_1-\Gamma_2)}\,\frac{F_{X,\,2}}{F_{X,\,1}} \sim 20\,. \qquad (2)$$

However, during the simultaneous Fermi observation, no significant γ-ray variability was observed for the analyzed sources, at least within one day timescale. Therefore, the remaining explanation for the observed X-ray spectral evolution is that the IC power-law slope remains roughly constant during the flux variations, but the amount of contamination from the additional soft X-ray component increases at low flux levels, affecting the spectral fitting parameters at higher photon energies ($> 2\,\mathrm{keV}$). Note that in such a case the expected gamma-ray variability should be of the same order as the X-ray variability, namely $F_{\gamma,\,2}/F_{\gamma,\,1} \simeq F_{X,\,2}/F_{X,\,1} \sim 1.3$.

We finally note in this context that, as shown in § 3.1.1, the previous BeppoSAX data for PKS 0208-512 collected during the high state indicated a convex X-ray spectrum, and an excess absorption below 1 keV with a column density of $N_\mathrm{H} \sim 1.67 \times 10^{21}\,\mathrm{cm^{-2}}$ exceeding the Galactic value by more than a factor of 5. However, the X-ray photon index was similar to the one implied by our Suzaku observations. Therefore, the convex spectrum observed by BeppoSAX may reflect an intrinsic shape of the IC emission involving the low-energy cut-off in the electron energy distribution around $\gamma \sim 1$, as expected in the EC/BLR model (Tavecchio et al. 2007), which is only diluted during the low-activity states due to the presence of an additional soft X-ray spectral component.

Interestingly, same trend has been observed in 3C 454.3 (Figure 2 (*right*)). Villata et al. (2006) reported $N_\mathrm{H} = (1.34 \pm 0.05) \times 10^{21}\,\mathrm{cm^{-2}}$ in the Chandra data collected in May 2005, during the outburst phase ($F_{2-8\mathrm{keV}} \sim 8.4 \times 10^{-11}\,\mathrm{erg\,cm^{-2}\,s^{-1}}$, which is ~ 5 times higher than in our observation). An even higher hydrogen column density was found by Giommi et al. (2006), when fitting the April-May 2005 data taken by the Swift XRT ($N_\mathrm{H} \sim 2 - 3 \times 10^{21}\,\mathrm{cm^{-2}}$). Since the synchrotron peak of each source is located around optical photon energies, the high-energy synchrotron tail may possibly account for the observed soft X-ray excess emission, especially if being modified by the Klein-Nishina effects (see the discussion in Sikora et al. 2009 and Kataoka et al. 2008). On the other hand, the bulk-Compton spectral component produced by Comptonization of the UV accretion disk by cold electrons in the innermost parts of relativistic jets (e.g., Begelman & Sikora 1987) is a natural explanation for the revealed soft X-ray excess component.

References

Abdo, A. A., et al. 2009a, ApJS, 183, 46
Abdo, A. A., et al. 2009b, ApJ, 700, 597
Abdo, A. A., et al. 2009c, ApJ, 699, 31
Abdo, A. A., et al. 2009d, submitted
Atwood, W. B., et al. 2009, ApJ, 697, 1071
Begelman, M. C., & Sikora, M. 1987, ApJ, 322, 650
Kataoka, J., et al. 2008, ApJ, 672, 787
Ghisellini, et al. 2009, arXiv:0906.2195
Giommi, P., et al. 2006, A&A, 456, 911
Poole, T. S., et al. 2008, MNRAS, 383, 627
Roming, P. W. A., et al. 2005, Spacs Sci. Rev., 120, 95
Sambruna, R. M., et al. 2006, ApJ, 652, 146
Sikora, M., et al. 2009, arXiv:0904.1414
Tavecchio, F., et al. ApJ, 665, 980
Villata, M., et al. 2006, A&A, 453, 817